Rapid antibiotic susceptibility test with characteristic patterns by combining an optically induced dielectrophoresis (ODEP)-based microchip system and artificial intelligence

Hsin-Yao Wang, MD[1*], Chia-Ru Chung, PhD[2], Zi-Ling Lin, MS[2], Min-Hsien Wu, PhD[1], Jang-Jih Lu, MD, PhD[1]

[1] Department of Laboratory Medicine, Chang Gung Memorial Hospital at Linkou, Taoyuan City, 33302, Taiwan

[2] Department of Computer Science and Information Engineering, National Central University, Taoyuan City, Taiwan

*Corresponding author: Hsin-Yao Wang, MD

E-mail: mdhsinyaowang@gmail.com

Highlights

- A novel microchip system can provide rapid (~2h) AST based on ODEP and AI
- Analysing bacteria with the ODEP light arrays confers characteristic AST patterns
- Accurate interpretation of the characteristic AST patterns is achieved by AI

Abstract

Precise antibiotic use for treating infectious diseases depends on antibiotic susceptibility test (AST). However, AST typically costs several days and significantly delays the precise antibiotics use. Rapid AST method is urgently needed. Optically induced dielectrophoresis (ODEP) is one of the promising technologies that can detect bacterial characteristics (e.g. antibiotic resistance) in a rapid and accurate manner. We developed an ODEP-based microchip system to provide rapid AST. Thirteen ODEP light arrays were designed to deliver a high resolution analysis. A various of representative bacteria and antibiotics were tested on the system. Bacterial strains were incubated in high concentration antibiotic solution for a short time (antibiotic shock) to enhance the difference between resistant and susceptible strains. Based on the antibiotic shock, the bacterial strains were analysed by the ODEP light arrays in the microchip and characteristic patterns of AST were generated. We applied artificial intelligence (AI) for an objective and accurate interpretation of the AST patterns. The results showed that the optimal time of antibiotic shock was < 2h. Resistant and susceptible strains showed characteristic spatial distribution over the 13 light arrays. The AI model could classify resistant strain from susceptible strain with accuracy > 0.99. In the study, we demonstrated that an ODEP-based microchip system combined with AI could provide rapid and accurate AST that would guide a more precise antibiotic use.

Keywords: antibiotic susceptibility test (AST); Optically induced dielectrophoresis (ODEP); artificial intelligence (AI)

Introduction

Infectious disease is one of the deadliest diseases causing considerable deaths annually worldwide. Death caused by infectious disease is estimated to proceed death of cancers by 2050 (Dadgostar, 2019). In the current battle against coronavirus disease 2019, humans are reminded of how weak we are when fighting infectious disease without effective drug. Thanks to the innovation of antimicrobial agent in 1940s, people cannot easily die from infectious diseases (Dadgostar, 2019). The lifespan has also extended significantly in the last decades. In the era of antibiotics, we are lucky that we do not have to fear of threat from infectious diseases too much. Unfortunately, we seem to run out of the "good luck" soon in the coming decades. Resistant rate against currently available antibiotics keeps growing. Moreover, emerging mechanisms of antibiotic resistance have been actively reported in recent year. In brief, we are running out of weapon against the pathogens. The fear of infectious diseases will come back to the world soon.

Inappropriate use of antibiotics is one of the major causes of antibiotic resistance. In clinical practice, adequate management and antibiotics administration for infectious diseases depends largely on conventional *in-vitro* antibiotic susceptibility test (AST) (Wang, H.Y. et al., 2018a). Typically, AST is determined by using paper disc, microdilution, E-test, etc (Wang, H.Y. et al., 2018a). Shortly, all of the current AST methods are based on the use of time-consuming bacteria culture for antibiotics testing. Therefore, the long

turn-around-time of the AST methods normally results in considerable delay for accurate disease treatment (Wang, H.-Y. et al., 2020b). Empirically, clinical physicians can only administer broad-spectrum antibiotics in managing the infectious diseases. In the period of empirical treatment, however, up to 50% cases could be falsely treated (Wang, H.-Y. et al., 2020b). In terms of epidemiology, higher rate and novel mechanism of antibiotic resistance can develop due to the falsely applied selection pressure came from inadequate antibiotics (Ventola, 2015).

Hence, a more rapid and accurate AST method is urgently in need. A variety of AST methods with different working mechanisms have been actively proposed. Electrochemical sensors were used for reporting rapid AST. Changes in impedance of the electrode-electrolyte interface reflected bacterial growth under certain antibiotics (Brosel-Oliu et al., 2019; Ward et al., 2018). Microfluidic chips were also developed for speeding AST up (Azizi et al., 2021; Xu, T. et al., 2021). AST could be tested in 3 h through concentrating bacteria cells in small scale in a microfluidic chip (Xu, T. et al., 2021). Microfluidic technique also could be used to create meticulous antibiotic gradients for testing AST in high resolution in 4h (Azizi et al., 2021). Following these AST methods, image analysis is typically applied for an automated and objective interpretation of analytical results (Xu, T. et al., 2021; Yu et al., 2018). Among these approaches, mass spectrometry (MS)-based method is considered to be the most rapid method, eliminating

the labor-intensive and time-consuming bacterial culture coming across in the conventional AST methods. Complex MS spectra include implicit information of AST (Wang, H.Y. et al., 2018a). Combined with artificial intelligence (AI), AST can be predicted at the same time of reporting bacterial species (Wang, H.Y. et al., 2020b). The abovementioned novel approach of AST has been successfully validated and demonstrated in different clinical settings (Wang, H.Y. et al., 2020b; Wang, Z. et al., 2020). Although rapid AST can be achieved, the accuracy of the MS-based AST method was around 90% (Wang, H.Y. et al., 2020b). The level of accuracy may not perfectly fit the clinical need sometimes where more accurate laboratory result is needed. Other MS-based studies determined AST by analyzing the metabolites of the antibiotics on MS spectra after short term incubating bacteria with antibiotic of interest (Welker and van Belkum, 2019). Accuracy of the approach was good but only specific antibiotic category (e.g. carbapenem) and specific resistant mechanism (e.g. carbapenemase) could be analyzed by the approach.

Technology of optically induced dielectrophoresis (ODEP) holds promise in providing rapid AST in clinical setting because it is accurate and cost-effective in manipulating cells. ODEP manipulates cells according to the electrical polarizability of cells without labelling. Single-cell level manipulation by ODEP provides a high resolution analysis of cells (Lin et al., 2009). Without complexed and expensive manufacture of physical electrodes, ODEP adopts light to generate virtual electrodes to conduct precise control of single cells. Cancer

cell strains with different properties of anti-cancer susceptibility can be discriminated by ODEP (Chu et al., 2019). For bacterial cells, which are largely different from mammalian cancer cells, ODEP technology has been used for detecting and isolating rare subpopulation of resistant bacteria from a bacterial mixture (Wang, H.-Y. et al., 2020a). In the applications, only short term pretreatment of cells by drugs is needed for the precise analysis (Chu et al., 2019; Wang, H.-Y. et al., 2020a). The culture-independent property of the approach renders ODEP a great potential to provide rapid AST.

ODEP typically manipulates cells with specific light modules and generates characteristic image patterns. With the advances of analytical methods, massive analytical data are produced. A comprehensive, objective, and unbiased interpretation of the data is not easy. Interpretation of the analytical results is highly vulnerable to person-to-person variation, and would results in medical error in the end. To address the issue, AI technology has raised considerable attention recently. The aforementioned studies also adopted AI in analyzing images (Yu et al., 2018) and MS spectra (Wang, H.Y. et al., 2020b) to predict AST. AI has been successfully applied in several clinical fields and outperforms traditional statistical methods (Lin et al., 2018; Tseng et al., 2019; Wang, H.-Y. et al., 2018; Wang, H.Y. et al., 2018a; Wang, H.Y. et al., 2020a; Wang et al., 2016; Wang, H.Y. et al., 2018b). On the basis of the outstanding analytical performance, harnessing AI algorithms in the difficult fighting against infectious diseases is reasonable. AI was used to enhance and standardize

the interpretation of the images (Yu et al., 2018). Applying AI in the analysis of ODEP results would be helpful in automated and objective interpretation.

Thus, we harnessed ODEP and AI technologies to develop and validate a novel diagnostic tool for rapid AST. Accurate and rapid AST of pathogens can help clinical physicians identify the culprit microorganism of the infectious diseases. Empirical use of antibiotics can be reduced and accurate antibiotics administration can be enhanced (Wang, H.-Y. et al., 2020b). Early and accurate administration of antibiotics by the novel ODEP-based tool would not only result in better prognosis for individual patients, but also diminish unnecessary selecting stress to pathogens so that resistance development could be limited.

2. Materials and methods

2.1 Scheme of the study

We aimed to utilize ODEP in discriminating bacteria with different properties of antibiotic susceptibility. The whole scheme is illustrated in Fig. 1(a). Before analysed by ODEP, bacteria strains (resistant and susceptible strains) were treated by high dose antibiotics for a short period ("antibiotic shock") to enhance the difference of electric property. The treated bacteria strains were analysed by ODEP and characteristic patterns (spatial distribution of single cells and aggregations) for antibiotic "resistant" or antibiotic "susceptible" were generated. Based on the analytical results of ODEP platform, we pre-processed and denoised the images of ODEP analysis prior to AI analysis. Following the pre-processing, single bacterial cells and bacterial aggregations could be discriminated. The patterns of either resistant or susceptible characteristics could be automated classified by AI algorithm.

2.2 Design of a microchip for ODEP-based AST

In this study, a simple microchip was designed for ODEP-based AST. The layout of the microchip is schematically illustrated in Fig. 2 (a). The microchip mainly encompassed a microchannel (L: 2.0 cm, W: 1.0 mm, and H: 30.0 μm). The ODEP-based cell analysis for AST was carried out at the analytical zone. One inlet hole and one outlet hole were located

147 over the both ends of the microchannel. The inlet hole was designed for loading suspended
148 bacterial sample, while the outlet hole was used for balancing the microfluidic body within
149 the microchannel. The structure of the microchip is schematically illustrated in Fig. 2 (b).
150 Shortly, the microchip is consisted of two customer-made polydimethylsiloxane (PDMS)
151 (Sylgard® 184, Dow Corning, USA) adapters for tubing connection (Layer A), an
152 indium-tin-oxide (ITO) glass (7 Ω, 0.7 mm; Ritek, Taiwan) (Layer B), double-sided
153 adhesive tape (DST-3, Sun-yieh, Taiwan; T: 30.0 μm) with the hollow structures of
154 microchannel and connecting holes (D: 1 μm) (Layer C), and a bottom ITO glass with a
155 coating layer of photoconductive material (composed by a 20-nm-thick n-type
156 hydrogenated amorphous silicon layer and a 1-μm-thick hydrogenated amorphous silicon
157 layer) (Layer D).
158
159 **2.3 Microfabrication and experimental setup**
160 We fabricated each layers of the microchip prior to assembling. The top PDMS
161 substrate (Layer A) was made by replica moulding process, in which details of preparation
162 were described in a previous study (Wu et al., 2013). For layer B, we drilled the ITO glass
163 to create the inlet hole and outlet hole by using a mechanical drill (26,000 rpm). For layer
164 C, we created a microchannel through the double adhesive tape by using manual punching.
165 For layer D, a series processes were used to create an amorphous silicon-coated ITO glass.

Briefly, an ITO layer with thickness of 70 nm was paved onto the glass to create an ITO glass. Based on high-density plasma chemical vapor deposition process, we then paved a n-type hydrogenated amorphous silicon (n-type a-Si:H) layer (T: 20 nm), followed by a hydrogenated amorphous silicon (a-Si:H) layer (T: 1 μm) onto the ITO glass. We used oxygen plasma surface treatment to pre-treat the surfaces of layer A and layer B, followed by bounding together. Layer B then bound with layer D through the adhesive property of layer C to complete the assembly of the microchip.

To utilize ODEP technology for rapid AST, the microchip was equipped together with other components to compose an ODEP-based microchip system. The components included a microchip, a function generator (AFG-2125, GW INSTEK, Taiwan), a commercial digital projector (PLC-XU350, SANYO, Japan), an operating computer, and a displaying computer. A charge-coupled device (CCD)-equipped microscope (Zoom160, OPTEM, USA) was used for real-time observation of analysis. The overall experimental setup is illustrated on Fig. 2(c).

2.4 Antibiotic shock for pre-treating bacteria

Antibiotic shock uses antibiotics to enhance the difference of the characteristics between resistant bacteria strain and susceptible bacteria strain. In the proof-of-concept study, we evaluated the performance of the ODEP-based microchip system on common

185 pathogens of clinical significance. *Escherichia coli* (the resistant strain: ATCC 35218 and
186 the susceptible strain: ATCC 25922) and *Staphylococcus aureus* (the resistant strain: Mu50
187 and the susceptible strain: BAA977) were used as the model micro-organisms for gram
188 negative pathogen and gram positive pathogen, respectively. The conditions of antibiotic
189 shock regarding incubation time and concentration of antibiotics were evaluated to
190 determine the optimal conditions for enhancing the difference between bacterial strains.

191 For *E. coli*, two commonly used antibiotics, Ampicillin (Merck, Germany) and
192 Unasyn (Ampicillin-sulbactam: Pfizer, USA) were evaluated; for *S. aureus*, Oxacillin and
193 Teicoplanin were evaluated. To evaluate the optimal conditions, antibiotic solutions were
194 prepared by serial titration. The antibiotic range for investigation were determined by the
195 minimal inhibitory concentrations (MICs) of the antibiotics (CLSI, 2020). Briefly, we
196 tested the candidate concentrations that may inhibit the susceptible strains but not the
197 resistant strains.

198 The final working concentrations of ampicillin were 200, 100, 50, and 25 μg/ml. For
199 Unasyn, the concentrations were 62.5, 31.25, 15.625, and 7.8125 μg/ml. For Oxacillin, the
200 concentrations were 50, 20, 10, and 5 μg/ml. For Teicoplanin, the concentrations were 10, 5,
201 2.5, and 1.25 μg/ml. We estimated bacterial growth by measuring OD600 at time of 0h,
202 0.5h, 1h, 1.5h, 2h, 3h and 6h. The condition (concentration and time) that rendered the
203 earliest difference of growth between the susceptible strains and the resistant strains were

considered as the optimal condition of antibiotic shock. Experiments for determining the optimal conditions of antibiotic shock were repeated in triplicate.

2.5 Working principle of ODEP-based AST

In the step of antibiotic shock, difference of bacterial characteristics between antibiotics resistant and susceptible strains were enhanced. We then applied a dynamic ODEP light module to analyse the bacterial strains (Fig. 3). We hypothesized that different characteristics of antibiotic susceptibility can be measured by ODEP. The different "ODEP-types" would discriminate antibiotics resistant strain from antibiotics susceptible strain. ODEP force exerted on bacteria follows the formula (Khoshmanesh et al., 2011)

$$\text{ODEP force} = \frac{\pi r^2}{3} L \varepsilon_0 \varepsilon_m \mathrm{Re}[f_{CM}] \nabla |E|^2 \qquad \text{formula 1}$$

where r, L, ε_0, ε_m, $\nabla|E|^2$, and $\mathrm{Re}[f_{CM}]$ are the bacterial width, bacterial length, vacuum permittivity, relative permittivity of the surrounding solution, gradient of the applied electrical field squared, and real part of the Clausius–Mossotti factor (f_{CM}), respectively (Wang, H.-Y. et al., 2020a). Under the same experimental settings for working solution and applied electrical field, ε_0, ε_m, $\nabla|E|^2$ would be the same for both resistant strain and susceptible strain of a specific species. Additionally, for a specific species, the size of bacteria is considered the same. We demonstrated that the bacterial length and width are not different between *E. coli* ATCC 35218 (Ampicillin resistant strain) and *E. coli* ATCC

223 25922 (Ampicillin susceptible strain) in our previous work (Wang, H.-Y. et al., 2020a).
224 Thus, the real part of the Clausius–Mossotti factor (f_{CM}) is considered as the only factor
225 that determines the degree of ODEP force. Re[f_{CM}] is associated with the polarizability of
226 the manipulated bacteria (Patel and Markx, 2008). Utilizing antibiotic shock, difference of
227 polarizability could be created when the permeability of plasma membrane is enhanced for
228 susceptible strains but not for resistant strain (Halder et al., 2015; Wang, H.-Y. et al.,
229 2020a). On the basis, ODEP-types could be analyzed and correlated well to the
230 characteristics of antibiotic susceptibility.

231 In the dynamic ODEP light module, we designed multiple light arrays with different
232 moving velocities to deliver analysis with high resolution. We applied the dynamic ODEP
233 light module to conduct a serial "spreading" of bacteria and create a characteristic pattern
234 of ODEP type (Fig. 3). The dynamic ODEP light module were composed of 13 light arrays
235 (20 μm x 20 μm squares). The moving velocities of the 13 light arrays were 0, 6.63, 13.65,
236 18.80, 24.50, 29.40, 36.70, 42.40, 48.00, 53.60, 59.40, 64.60, 69.90, and 75 μm/s. Different
237 moving velocity of light indicates different hydrodynamic drag force for manipulated
238 bacteria. The hydrodynamic drag force of moving bacteria follows Stokes' law (Ohta et al.,
239 2007):

240 $$F = \frac{6\pi r\eta}{\ln\left(\frac{r}{L}\right)}v \qquad \text{formula 2}$$

241 where L and r are the diameters of the long and short axes of bacteria, respectively; η and v

are the viscosity of the fluid and the maximum velocity of a cell, respectively (Wang, H.-Y. et al., 2020a). For manipulated bacteria in ODEP solution, the ODEP force balances the hydrodynamic drag force. Based on the formula 1 and formula 2, the moving velocity of the bacteria could be correlated to the bacterial characteristics of antibiotic susceptibility.

2.6 Analysis on the ODEP-based microchip system

In the ODEP-based microchip system (Fig. 2(c)), a uniform electric field was generated in the solution between the two ITO glasses (Layer B and Layer D, Fig. 2 (b)) through an AC electrical voltage (8 V, 600 KHz) between them. In this situation, the micro-scale particles (e.g., bacteria) suspended in the solution layer sandwiched in between the ITO glasses were electrically polarized. When the on the ITO glass with photoconductive material [Layer D, Fig. 2 (b)] was projected with light, it caused the decline of electric voltage across the solution layer within the light-projected zone, and generated a non-uniform electric field within the ODEP microchip. The light-induced local non-uniform electric field provides the basis of manipulating polarized bacteria (Fernandez et al., 2017).

In the step of antibiotic shock, SYTO 9/PI was used as a cell viability assay to pre-stain the bacteria (Thermo Fisher Scientific, CA, USA). Bacteria cells with high cell viability would emit greenish fluorescence, and bacteria with low cell viability would emitted reddish fluorescence in dark field. Before the analysis in the ODEP microchip, solution exchange to low conductivity (2 to 5 μs/cm) is necessary for a successful ODEP operation

(Wang, H.-Y. et al., 2020a). After antibiotic shock, we conducted solution exchange (centrifuging at 6,000 g for 5 min followed by re-suspending pellet in a sucrose solution (103 mg/ml)) for three times. The working sucrose solution were then injected into the ODEP microchip. In the analytical zone of the ODEP microchip, we designed 13 different light arrays with different moving velocities for the dynamic ODEP light module. We applied the dynamic ODEP light module to conduct a serial "spreading" of bacteria and create a characteristic pattern of ODEP type (Fig. 3). The 13 light arrays moved in descending order of velocity from the left (origin) to the right (end) of the analytical zone on the microchip (Fig. 3; Supplemental video). Theoretically, bacterial cells with the highest integrity of plasma membrane would be firstly dragged by the first (fastest) light bar. Bacterial cells with relatively lower integrity of plasma membrane were dragged by the second light bar, and so on. The whole process of analysis was recorded as video.

2.7 Data pre-processing for the analyses prior to AI-aided classification

Pre-processing of the recorded videos aims to de-noise the image prior to automated classification by AI. After injecting the sample solution in to the ODEP microchip, we applied several light arrays to reset the bacteria to the origin of the analytical zone (Fig. 3). However, some non-specific adhesions of bacteria may be still possible even after the resetting operation. The initial image prior to ODEP analysis was stored as background

(JPG format, b1, Fig. 4). Median filtering method was used for eliminating the noise (George et al., 2018). Specifically, a sliding window with size of 441 pixels was sliding through the whole area of the background (b1, Fig. 4). Within each window, median values of the pixels (in RGB grayscale) were calculated and used to impute for the pixel whose value was higher than median. The difference between the filtered image (b2, Fig. 4) and the background (b1, Fig. 4) was calculated (supplemental Fig. 1), and the coordinates of the differences were considered as the noises (b3, Fig. 4). The final image of analysis video was stored (a, Fig. 4), and opencv library was used for HSV color space (b, Fig. 4) (Smith, 1978). Through range of the HSV color space chosen, only areas of light arrays were picked up. The average grayscale value of the light arrays was used to replace the noises according to the coordinates of the noises (supplemental Fig. 2). The remaining objects in the light arrays were regarded as the target cells (c, Fig. 4). To define the objects, we applied canny algorithm to find the greyscale value gap and define the boundary of the objects (Rong et al., 2014).

On the basis of the target cells, a further discrimination of “single cell” and “aggregation” was conducted for a more meticulous characterization of antibiotic susceptibility. After antibiotic shock, some bacterial cells could stay in the phenotype of single cell. The others would aggregate together, and annotated as “aggregation” in the study. Bacteria with antibiotic resistance would more likely stay in single cell phenotype,

while bacteria without antibiotic resistance tend to aggregate together (Corno et al., 2014; Haaber et al., 2012). Single cell was defined when the size of the objects was smaller than 150 pixels. By contrast, aggregation was defined when area of pixels was larger 150.

2.8 AI-aided classification of antibiotic susceptibility

The spatial distribution of single cells and aggregations were used as the input for the AST AI. Based on the light arrays design, there were 13 light arrays with different moving velocities. Thus, there were 13 input features for the data of single cells and the other 13 input features for the data of aggregations. In total, 26 input features were used as the input features.

We used random forest (RF) as the AI algorithm for AST classification. RF is an ensemble algorithm that integrate multiple decision tree to deliver classification. Each decision tree in RF randomly selects a subset of k features from training dataset (totally m features). Majority voting of predicted labels is used for determination of classification. In this study, "randomForest" package in R was applied to construct RF classifiers based on various feature subsets (Liaw and Wiener, 2002). Synthetic minority over-sampling technique (SMOTE) was used for oversampling of the samples (Chawla et al., 2002). Three-fold cross validation was used for evaluating the performance of classification.

3. Results

3.1 Optimal condition of antibiotic shock

The aim of antibiotic shock is to enhance the difference of polarizability between susceptible and resistant bacterial strains. Meanwhile, to speed up the time spent on the step of antibiotic shock, we evaluated the optimal time and concentration of antibiotic shock. For ampicillin on *E. coli*, concentrations that ranged from 25 to 200 μg/ml were investigated (Fig. 5(a)). When the concentrations were 25, 50, and 100 μg/ml, the growth *E. coli* ATCC 25922 (susceptible strain) was not suppressed further than *E. coli* ATCC 35218 (resistant strain) in short period of incubation time. On 200 μg/ml, the growth of *E. coli* ATCC 25922 was suppressed sharply while *E. coli* ATCC 35218 (resistant strain) was not suppressed shortly after 1 h antibiotic shock. Thus, the optimal condition for ampicillin on *E. coli* was determined as 200 μg/ml for 1 h. For Unasyn on *E. coli*, the result revealed that 31.25 μg/ml for 1.5 h was the optimal condition (Fig. 5(b)). For *S. aureus*, optimal conditions of antibiotic shock for oxacillin and teicoplanin were 5 μg/ml for 1 h, and 2.5 μg/ml for 1h, respectively(Fig. 5(c) and Fig. 5(d)).

3.2 Analysis of bacteria with different properties of antibiotic susceptibility on the ODEP-based microchip system

After the antibiotic shock, the difference of polarization between resistant and

338 susceptible strains was enhanced. We injected the treated bacteria and used the
339 ODEP-based microchip system to analyze the bacterial strains. Without antibiotic shock
340 (negative control), both resistant strain and susceptible strain distributed mainly over the
341 high velocity zones (right part of the microchip) (Fig. 6(a) and Fig. 6(b)). No difference of
342 spatial distribution between resistant and susceptible strains was noted. Moreover, green
343 spots were noted for both resistant and susceptible strains, indicating high cell viability.

344 For the bacterial strains were treated by ampicillin (Fig. 6(a)), *E. coli* ATCC 35218
345 (resistant strain) still distributed over the high velocity zones and revealed high cell
346 viability. Meanwhile, *E. coli* ATCC 25922 (susceptible strain) distributed sparsely over the
347 microchip. Moreover, larger spots with yellowish color were noted for *E. coli* ATCC 25922.
348 The larger spots were considered as “aggregation” in the study. For the bacterial strains
349 were treated by ampicillin-sulbactam (Fig. 6(a)), similar spatial distribution was noted.
350 However, *E. coli* ATCC 35218 turned reddish color, indicating low cell viability.

351 For *S. aureus* Mu50 (resistant strain), bacterial cells distributed majorly over the high
352 velocity zones in either negative control, oxacillin treatment, and teicoplanin treatment (Fig.
353 6(b)). *S. aureus* Mu50 emitted greenish color in both negative control and oxacillin
354 treatment groups, but emitted yellowish color in teicoplanin treatment group. *S. aureus*
355 BAA-977 (susceptible strain) distributed sparsely over the microchip in both oxacillin and
356 teicoplanin treatment groups. *S. aureus* BAA-977 showed yellowish color in oxacillin

group, and reddish color in teicoplanin group, indicating decreased cell viability under antibiotic shock.

3.3 Pattern of antibiotic susceptibility classified by AI

On the basis of the analyses, specific patterns on the microchip were representative of the antibiotic susceptibility. The analytical results of various conditions were summarized according to the spatial distribution of single cells and distributions (Fig. 7). In brief, resistant strains distributed over high velocity zones and susceptible strains distributed sparsely for either *S. aureus* (Gram positive bacteria) or *E. coli* (Gram negative bacteria). More aggregations were noted for susceptible strains than resistant strains.

The characteristic patterns could be easily interpreted by human operators. Furthermore, to enhance the objectivity and consistency of interpretation, we applied RF algorithm for an automated interpretation of the patterns. Using the spatial distribution of single cells and aggregations as the input, the RF model performed sensitivity at 0.992 (standard deviation: 0.017) and specificity at 0.992 (standard deviation: 0.018). The performance of AST classification was high and stable for robustly deliver an objectively automated interpretation.

4. Discussion

In the proof-of-concept study, we demonstrated that the ODEP-based microchip system could provide rapid AST in high resolution. Based on the dynamic ODEP light module that was composed of 13 different light arrays, characteristic patterns were generated for specific AST properties. Moreover, harnessing AI would render the interpretation of AST rapid, accurate, and objective. We demonstrated the ability of the system in discriminating resistant strain from susceptible strain for important clinical pathogens and commonly used antibiotics. The AI-aided ODEP-based microchip system is a promising analytical tool to provide more rapid and accurate AST that is capable of guiding a more appropriate antibiotics use and leading to a more favorable clinical outcome for infectious diseases.

Antimicrobial resistance (AMR) has been growing since first antibiotic were discovered and used. Heterogeneity is considered as one of the major causes of growing AMR and treatment failure (Mikkaichi et al., 2019; Zheng et al., 2020). Minor resistant bacteria may account only a very small part of an isolate (Wang, H.Y. et al., 2018a). For detecting such a rare minority that is overwhelmed by majority, an analytical tool with high resolution is necessary. Microdilution method, which is the gold standard method of AST, applied serial dilutions to measure the antibiotic MICs. The gap between two dilution titers (e.g. 8 μg/ml and 16 μg/ml) would be too large to determine the precise MIC. Moreover, either solution-based (e.g. microdilution, macrodilution) or agar-based (e.g. paper disc

394 diffusion) AST methods primarily depends on observation of gross phenotype. Subtle
395 difference existing in an isolate with heterogeneous property would not be detectable by
396 using the conventional AST methods. By contrast, in a previous work we demonstrated that
397 ODEP-based microfluidic chip can detect the heterogeneous property even when the minor
398 group is very rare (10^{-3}) (Wang, H.-Y. et al., 2020a). Taking the ability of ODEP in
399 manipulating single cells further, we designed 13 velocity zones with different level of
400 manipulating force. The design would provide a AST with higher resolution than traditional
401 AST methods. The correlation between the ODEP-based AST and MICs or clinical
402 outcomes are worthy of further investigation.

403 Rapid turnaround time is crucial in managing infectious diseases. In COVID-19
404 pandemic, the turnaround time of a test is even more important than its sensitivity
405 (Larremore et al., 2021). Conventional AST methods typically cost more than 16 h to report
406 AST, and the considerable delay would result in unfavorable outcomes. Thus, reducing the
407 turnaround time of the ODEP-based AST is the other key in additional to its high resolution.
408 We applied antibiotic shock to pre-treat bacteria strains prior to analysis by ODEP
409 microchip. The idea of antibiotic shock is elevating the concentration of antibiotic as
410 possible and shortening the turnaround time of AST. Through antibiotic shock, we could
411 reduce the turnaround time from more than 16 h to 1-2 h (Fig. 5). The culture based AST
412 method or cell viability test by using SYTO 9/PI staining cannot discriminate resistant

413 strain from susceptible strain after the antibiotic shock. In the groups of *E. coli*
414 (ampicillin-sulbactam) (Fig. 6(a)) and *S. aureus* (teicoplanin) (Fig. 6(b)), both resistant
415 strain and susceptible strain showed yellowish/reddish signals. In brief, we could not detect
416 antibiotic resistance based on neither culture nor the staining results. By contrast, the
417 resistant strains (*E. coli* ATCC 35218 and *S. aureus* Mu50) revealed characteristic patterns
418 from the susceptible strains (*E. coli* ATCC 25922 and *S. aureus* BAA-977) on the ODEP
419 microchip (Fig. 6). The results indicated that ODEP would be a more sensitive method than
420 culture or viability test to detect antibiotic resistance after a short turn antibiotic shock.

421 AI technology was used to provide a rapid, objective, and accurate interpretation of the
422 characteristic patterns. Specifically, RF instead of deep learning was used in the study. RF
423 is a classical algorithm that has proven its utility in the community of microbiology (Lin et
424 al., 2018; Wang, H.Y. et al., 2020b; Xu, J. et al., 2021). The high interpretability of RF
425 renders it a popular algorithm in medical field in which reasons behind AI predictions are
426 essentially required. Moreover, RF algorithm is one of the most energy effective algorithms
427 in dealing with clinical laboratory data (Yu et al.). In the clinical practice of most clinical
428 microbiology laboratories, only standard personal computer is equipped. High level CPU
429 and RAM are typically unavailable, so as GPU that is used for efficient deep learning. In
430 brief, the computation resources in most clinical microbiology laboratories are limited. RF
431 would be the practical AI algorithm in the real-world situation. With RF algorithm, training

and deployment are available on standard personal computers. Moreover, based on the property of energy efficiency, integrating the ODEP-based microchip system and the computation hardware together as an all-in-one device is possible and promising.

In the proof-of-concept study, we would like to acknowledge several limitations. First, several representative bacteria strains and important antibiotics were investigated. To develop a clinically useful diagnostic tool, more bacteria strains and more antibiotics should be tested to construct the optimal condition of antibiotic shock, database of the AST patterns, and the AI models. Second, standard bacteria strains with steady MICs were used in the study. Clinical bacteria strains with large range of MICs are worthy of further investigation. The last, ODEP-based microchip system could provide AST in high resolution. However, the correlation of the high resolution AST and conventional MICs are still unknown. Moreover, clinical relevance and impact of the high resolution AST is of interest. Theoretically, a higher resolution AST would lead to a more precise antibiotics use. on the other aspect, it is also possible that semi-quantitative or even qualitative AST methods may be useful enough for managing infectious diseases in clinical settings.

Conclusions

We developed an AI-aided ODEP-based microchip system that able to provide rapid AST, and validated its utility by using representative bacteria and antibiotics. Characteristic patterns of resistant and susceptible strains were found on the ODEP analysis, and the patterns could be automatedly interpreted by a RF model. The rapid AST would be beneficial in early prescription of adequate antibiotics and patients' outcome.

Acknowledgements

This work was sponsored by the Ministry of Science and Technology, R.O.C. (MOST 105-2221-E-182-028-MY3 and MOST 104-2628-E-182-002-MY3) and Chang Gung Memorial Hospital (CMRPD2E0011-13, CMRPD2G0061-62, and CMRPD2H0121).

Competing financial interests

The authors declare no competing financial interests.

Figure captions

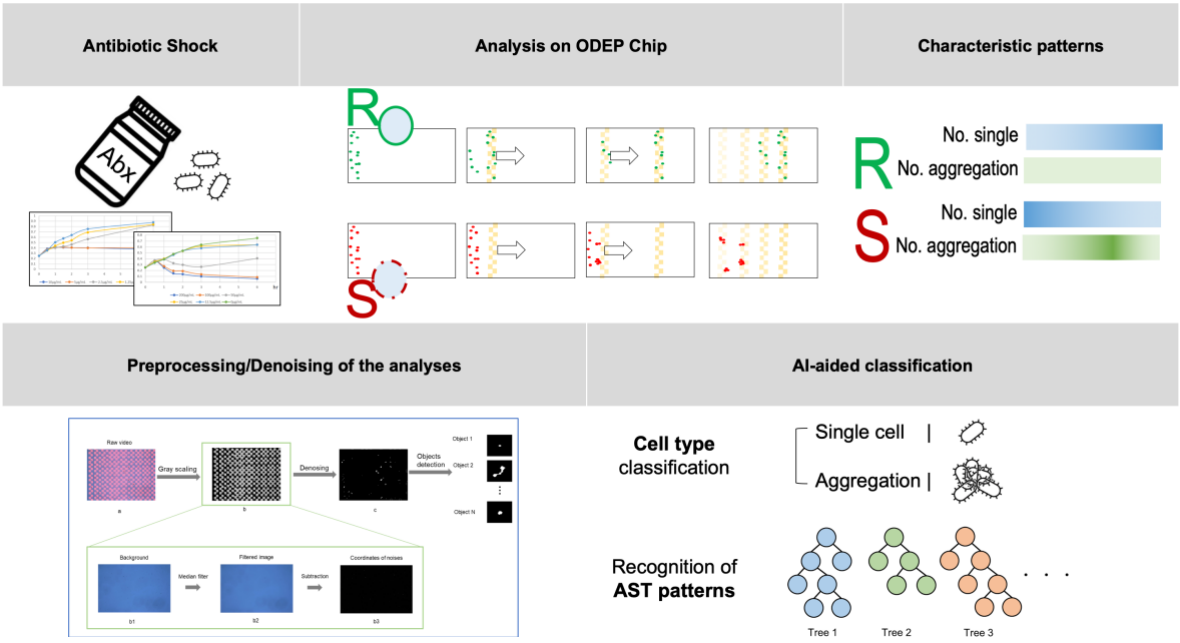

Fig. 1 Study design. The ODEP-based microchip system can be divided into four major steps, including antibiotic shock, analysis on ODEP chip, generating characteristic AST patterns, preprocessing the analyses, and AI-aided classification of AST patterns. In the step of antibiotic shock, high concentration antibiotics are used to enhance the difference of electric property between resistant and susceptible strains in a short period. ODEP light arrays are used to analyze the bacterial strains after the antibiotic shock. Characteristic AST patterns for resistant or susceptible strains are generated in the ODEP microchip. For an automated and objective interpretation of the AST patterns, AI algorithm is applied. Prior to AI-aided interpretation, preprocessing of the analytical measurements are adopted. Lastly, the AST AI can robustly provide a high resolution AST automatically. ODEP: optically induced dielectrophoresis. AST: antibiotic susceptibility test. AI: artificial intelligence.

Figure 2(a).

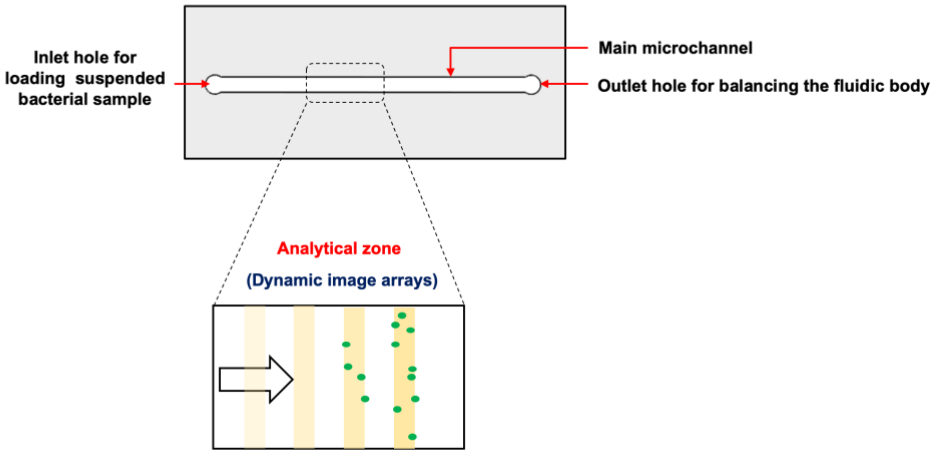

477

Figure 2(b).

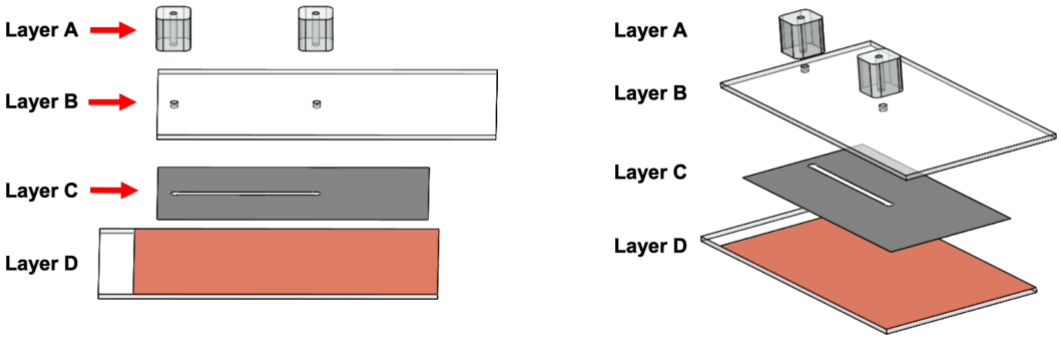

478

Figure 2(c).

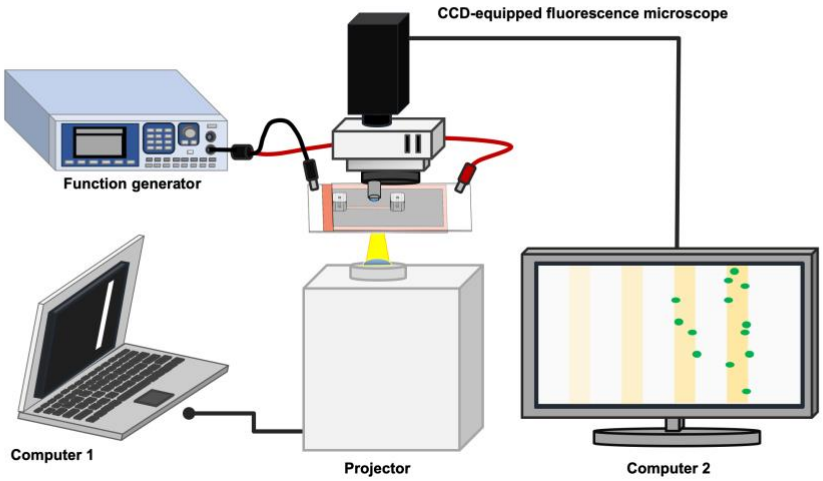

Fig. 2 Design of the ODEP microchip. (a) Top view: A relatively simple design is applied to carry out the conduct the ODEP-based AST. The ODEP microchip is composed of a main microchannel. An inlet hole is design at one end of the main microchannel, while an outlet hole is located at the other end. In the middle of the microchannel, an analytical zone is designed for conducting the ODEP-based AST. (b) Explosive view: The ODEP microchip is composed of four layers. The layer A is a polydimethylsiloxane connector. The layer C is an adhesive tape adhering layer B (ITO glass) and layer D (ITO glass coated with photoconductive material). (c) Experimental setting: The ODEP microchip is located at the center of the ODEP-based system, connected with a functional generator. Computer 1 is used for controlling the ODEP light module that is generated by the projector, while computer 2 is connected with CCD-equipped microscope to inspect the process of analysis. ODEP: optically induced dielectrophoresis. AST: antibiotic susceptibility test. ITO: indium-tin-oxide. CCD: charge-coupled device.

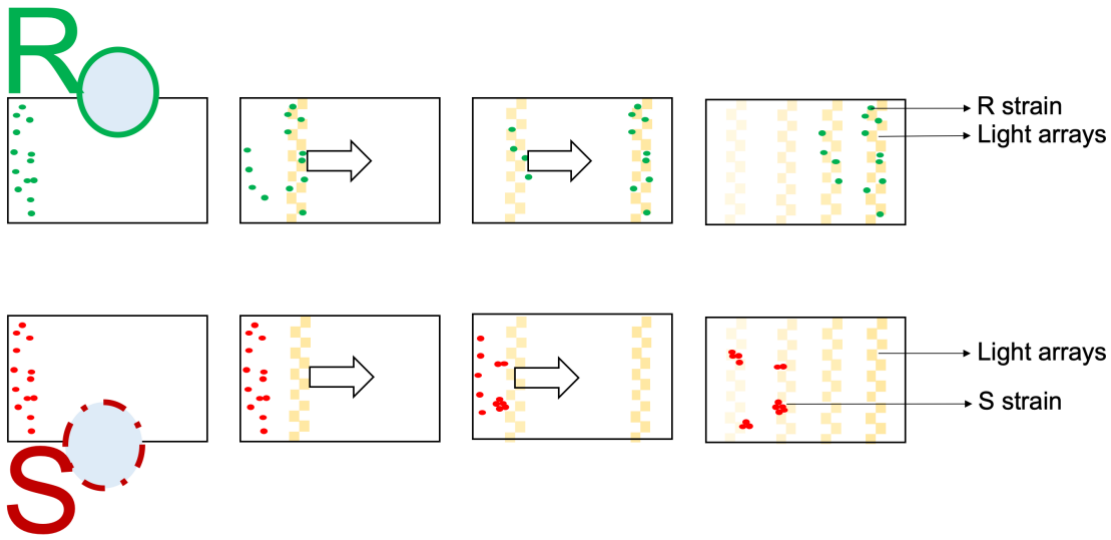

Fig. 3 Characteristic AST patterns. The figures illustrate characteristic patterns would be generated by the ODEP-based microchip system. We design an ODEP light module that is composed by different light arrays. The light arrays move with different moving velocities, indicating a various of ODEP forces are generated by the light arrays. In the microchip, the light arrays move based on the descending order of moving velocity. Resistant strain (R) that maintains higher polarizability would be carried to the right part (high speed zone) of the microchip by the light arrays with higher velocity. By contrast, susceptible strain (S) would not be spread thorough the microchip and stay in the left part (low speed zone) of the microchip. The characteristic patterns can be used to discriminate the resistant strain from susceptible strain. ODEP: optically induced dielectrophoresis.

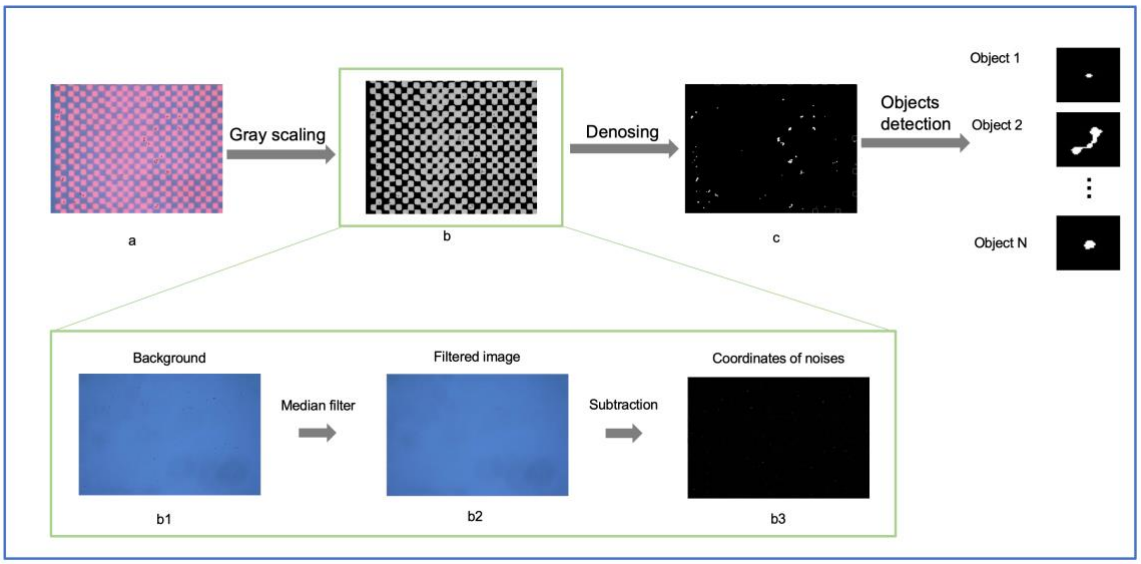

Fig. 4 Preprocessing of the analytical results. The ODEP analysis is recorded as video. For a more robust AI-aided automated interpretation of the analytical results, the analytical results are preprocessed. First, the initial frame (background, b1) and the end frame (a) of the video are saved. Median filter method is used for identifying the coordinates of the noises in the image of background (b1). We can get image b through gray scaling image a. Through comparing b and b3, denoising is operated and the left are the target objects. The objects are detected and their spatial distribution are recorded for further interpretation of characteristic patterns. ODEP: optically induced dielectrophoresis.

Figure 5(a).

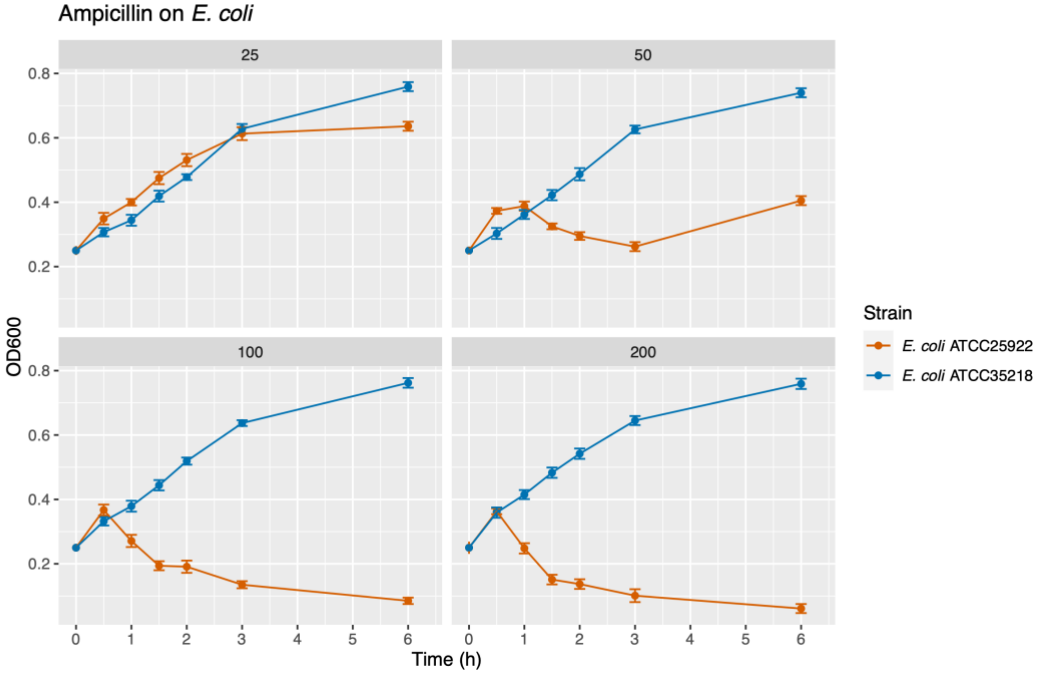

516

Figure 5(b).

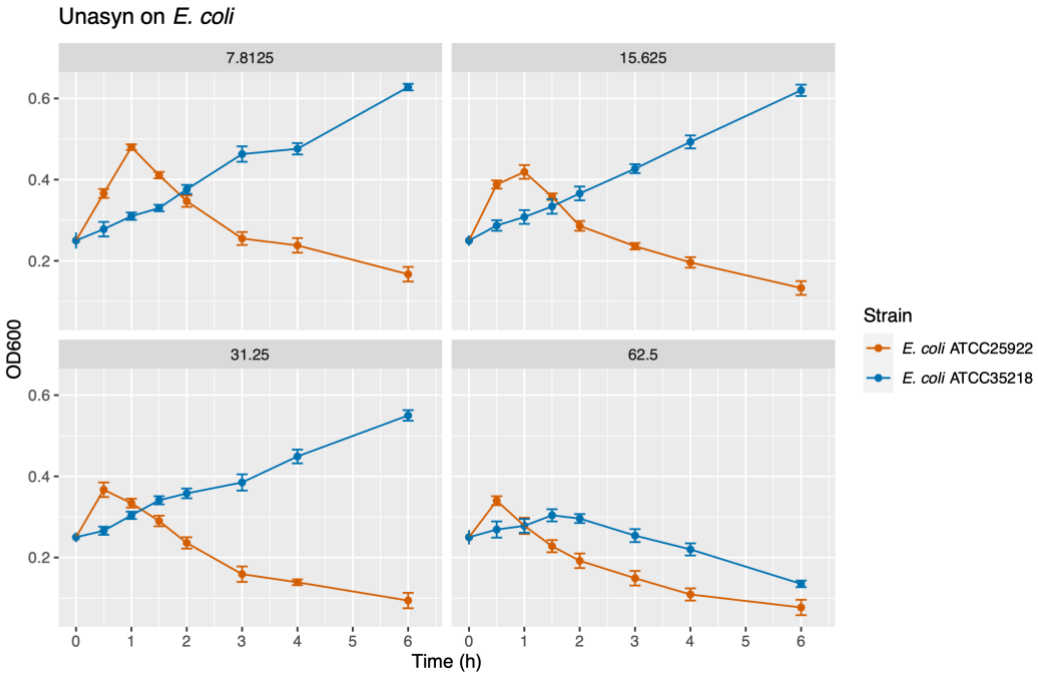

517

Figure 5(c).

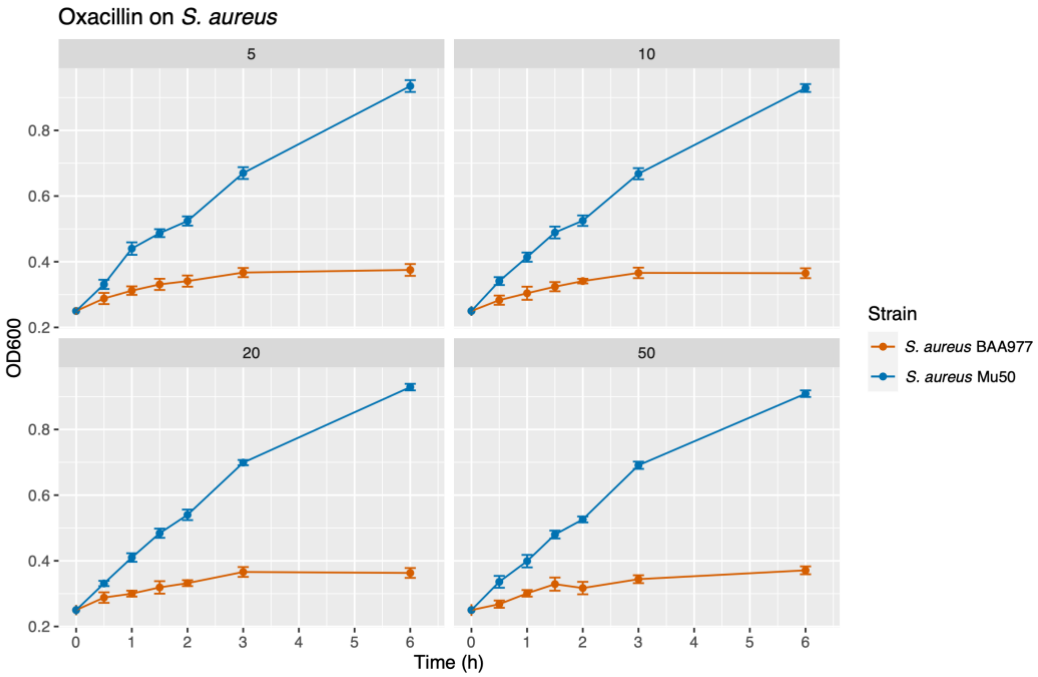

518

Figure 5(d).

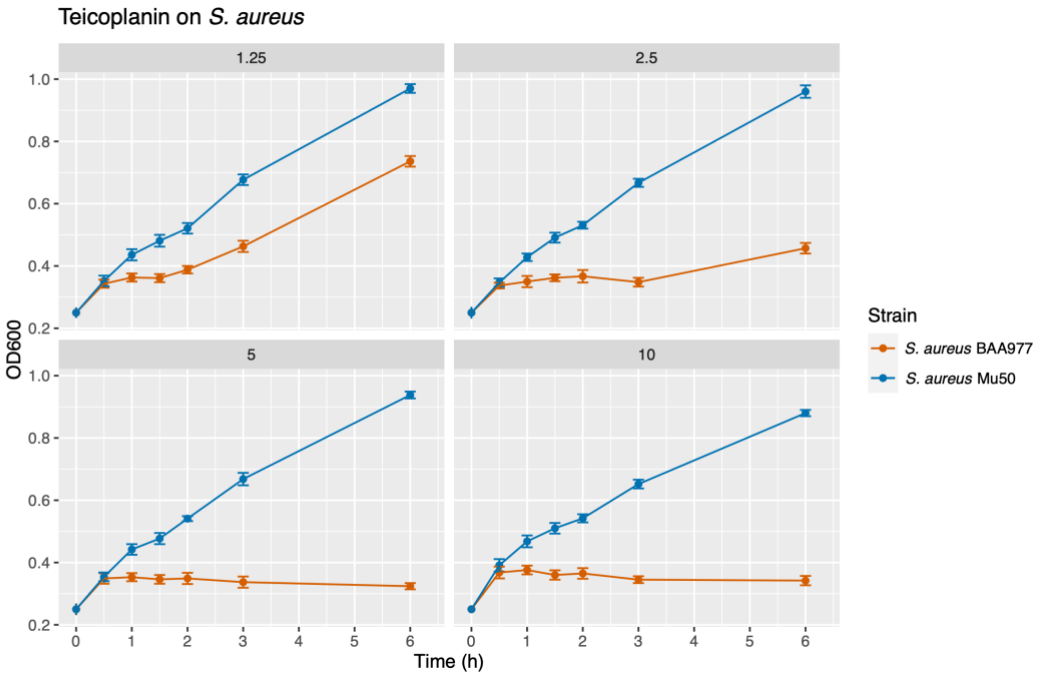

519

520 **Fig. 5 Optimal conditions of antibiotic shock.** Antibiotic shock is used the enlarge the
521 difference of polarizability between resistant and susceptible bacterial strains. The
522 experiments determine the optimal conditions that suppress susceptible strains
523 while not suppress resistant strain. **(a) Ampicillin on *E. coli***: Conditions of 25, 50,
524 100, and 200 μg/ml are investigated. The results show that 200 μg/ml for 1 h is the
525 optimal condition. (b) **Unasyn (ampicllin-sulbactam) on *E. coli***: The optimal

condition is 31.25 μg/ml for 1.5 h. (c) **Oxacillin on *S. aureus*:** The optimal condition is 5 μg/ml for 1 h. (d) **Teicoplanin on *S. aureus*:** The optimal condition is 5 μg/ml for 1 h.

Figure 6(a).

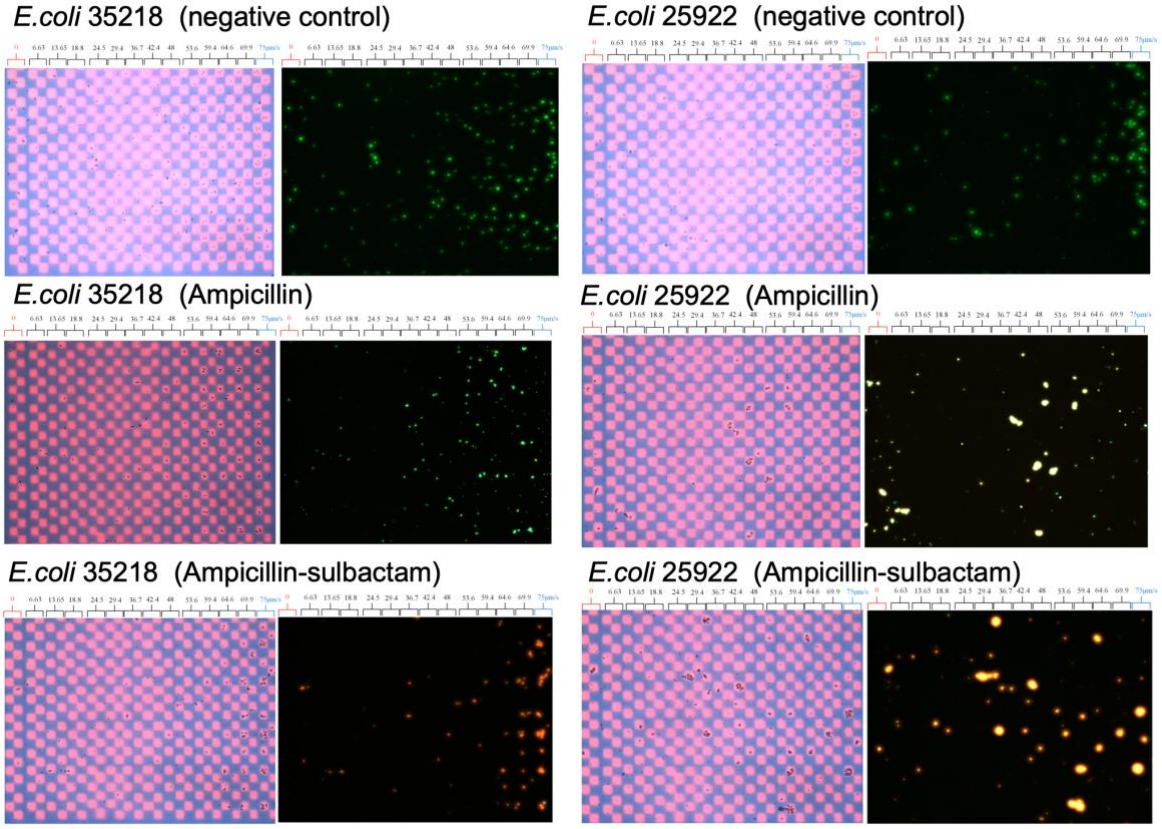

529

Figure 6(b).

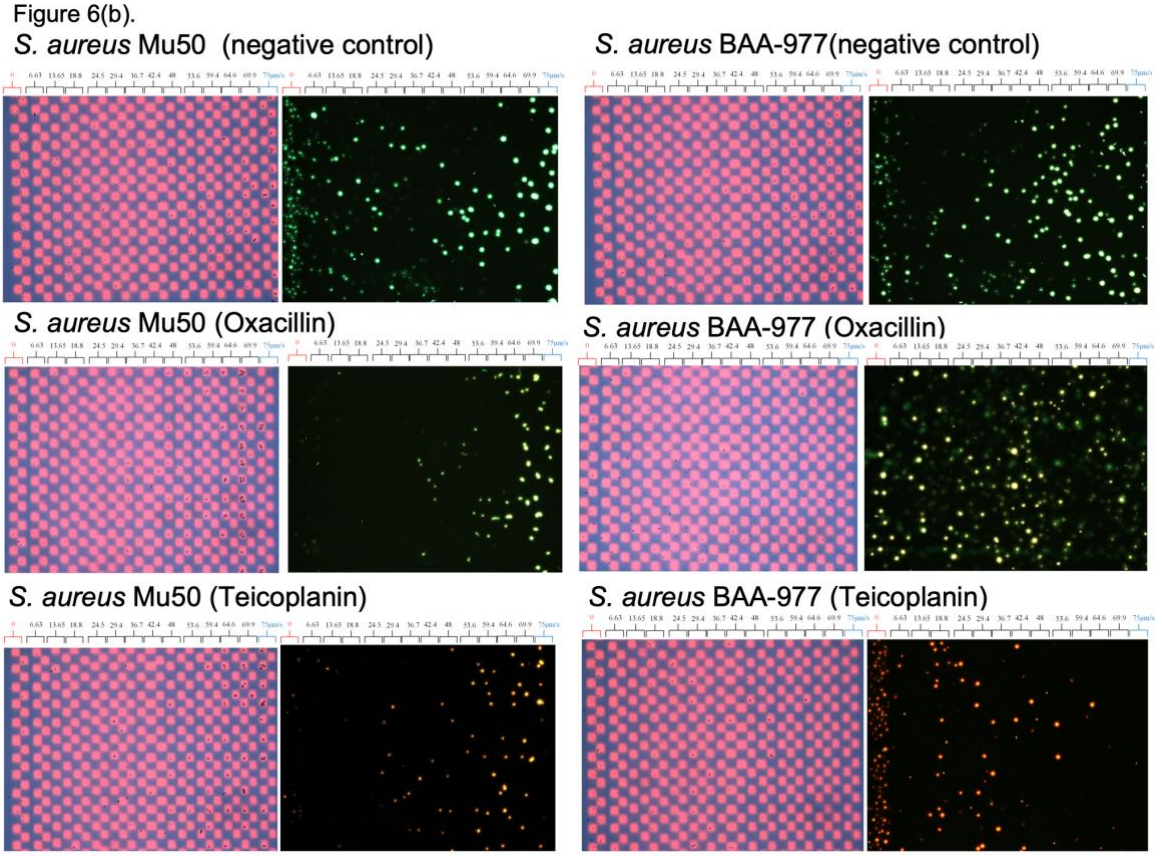

530

Fig. 6 ODEP analysis of bacteria strains that treated with different antibiotics. (a) *E. coli* is used as the reportative microorganism for gram negative pathogen. *E. coli* ATCC 35218 is used as the model microorganism of resistant strain, while *E. coli* ATCC 25922 is used as the model microorganism of susceptible strain. In the negative controls, both *E. coli* ATCC 35218 and *E. coli* ATCC 25922 show similar spatial distribution in which most bacteria distribute over the right part (high speed zone). Besides, both *E. coli* ATCC 35218 and *E. coli* ATCC 25922 reveal greenish fluorescence in dark field. In the ampicillin group, *E. coli* ATCC 35218 distributes over high speed zone while *E. coli* ATCC 25922 distributes sparsely. In the dark field, *E. coli* ATCC 35218 reveals greenish fluorescence but it is yellowish for *E. coli* ATCC 25922. In the ampicillin-sulbactam group, *E. coli* ATCC 35218 distributes over high speed zone while *E. coli* ATCC 25922 distributes sparsely. In the dark field, *E. coli* ATCC 35218 reveals reddish fluorescence and *E. coli* ATCC 25922 reveals orange fluorescence. (b) *S. aureus* is used as the representative microorganism for gram positive pathogen. *S. aureus* Mu50 is used as the model microorganism of resistant strain, while *S. aureus* BAA-977 is used as the model microorganism of susceptible strain. In the negative controls, both *S. aureus* Mu50 and *S. aureus* BAA-977 show similar spatial distribution and fluorescence. In the oxacillin group, *S. aureus* Mu50 distributes over high speed zone while *S. aureus* BAA-977 distributes sparsely. The fluoresce for *S. aureus* Mu50 and *S. aureus* BAA-977 are green and yellow, respectively. In the teicoplanin group, *S. aureus* Mu50 distributes over high speed zone and emits yellowish fluorescence. In contrast, *S. aureus* BAA-977 distributes over low speed zone and emits reddish fluorescence. ODEP: optically induced dielectrophoresis.

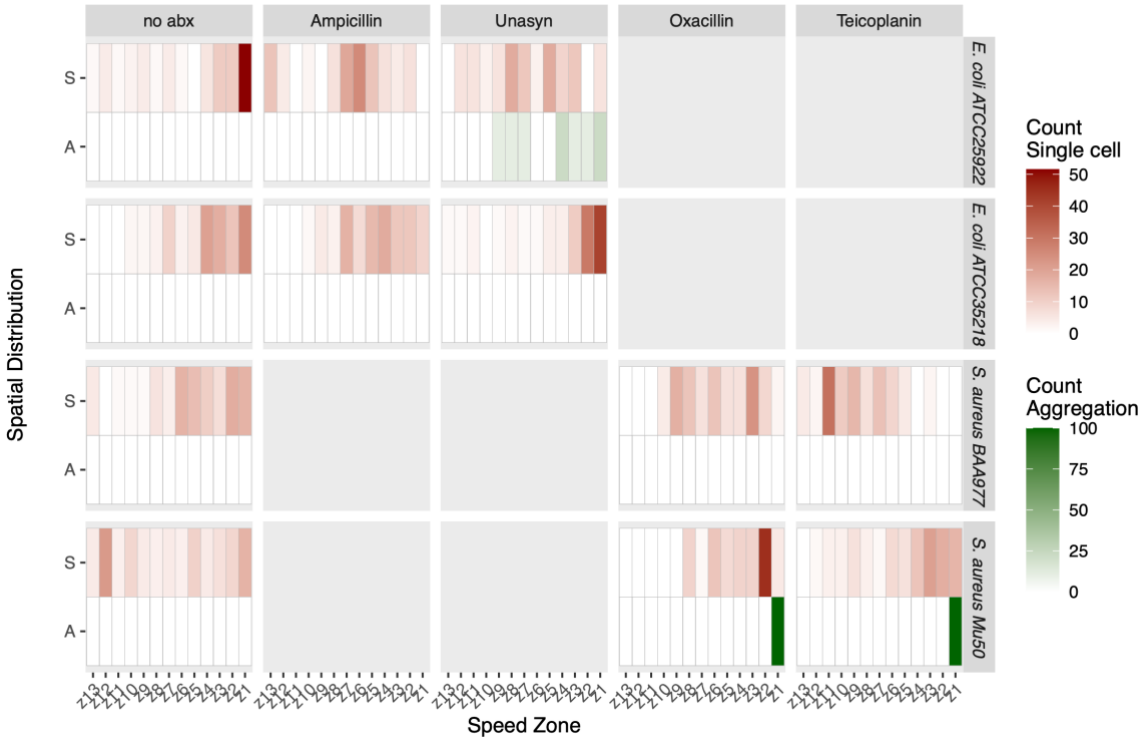

Fig. 7 Illustration of the characteristic AST patterns for different pathogens treated with different antibiotics. The spatial distributions of single cells and cell aggregations amid different conditions are demonstrated. In the study, totally 13 light arrays with different moving velocities are designed, indicating 13 different speed zones. For resistant strains (*E. coli* ATCC 35218 and *S. aureus* Mu50), bacterial cells majorly distribute over high speed zones. By contrast, for susceptible strains (*E. coli* ATCC 25922 and *S. aureus* BAA-977), the characteristic pattern is a spare distribution of single cells and aggregations. AST: antibiotic susceptibility test.

Video Clip 1: The dynamic process of analyzing *E. coli* ATCC 35218 and *E. coli* ATCC 25922 by the ODEP light arrays. ODEP: optically induced dielectrophoresis.

References

Azizi, M., Davaji, B., Nguyen, A.V., Zhang, S., Dogan, B., Simpson, K.W., Abbaspourrad, A., 2021. Gradient-Based Microfluidic Platform for One Single Rapid Antimicrobial Susceptibility Testing. ACS Sens 6(4), 1560-1571.

Brosel-Oliu, S., Mergel, O., Uria, N., Abramova, N., van Rijn, P., Bratov, A., 2019. 3D impedimetric sensors as a tool for monitoring bacterial response to antibiotics. Lab Chip 19(8), 1436-1447.

Chawla, N.V., Bowyer, K.W., Hall, L.O., Kegelmeyer, W.P., 2002. SMOTE: Synthetic Minority Over-sampling Technique. Journal of Artificial Intelligence Research 16, 321-357.

Chu, P.-Y., Liao, C.-J., Hsieh, C.-H., Wang, H.-M., Chou, W.-P., Chen, P.-H., Wu, M.-H., 2019. Utilization of optically induced dielectrophoresis in a microfluidic system for sorting and isolation of cells with varied degree of viability: Demonstration of the sorting and isolation of drug-treated cancer cells with various degrees of anti-cancer drug resistance gene expression. Sensors and Actuators B: Chemical 283, 621-631.

CLSI, 2020. Performance Standards for Antimicrobial Susceptibility Testing. 30th ed. CLSI supplement M100. Wayne, PA: Clinical and Laboratory Standards Institute.

Corno, G., Coci, M., Giardina, M., Plechuk, S., Campanile, F., Stefani, S., 2014. Antibiotics promote aggregation within aquatic bacterial communities. Front Microbiol 5, 297.

Dadgostar, P., 2019. Antimicrobial Resistance: Implications and Costs. Infect Drug Resist 12, 3903-3910.

Fernandez, R.E., Rohani, A., Farmehini, V., Swami, N.S., 2017. Review: Microbial analysis in dielectrophoretic microfluidic systems. Anal Chim Acta 966, 11-33.

George, G., Oommen, R.M., Shelly, S., Philipose, S.S., Varghese, A.M., 2018. A Survey on Various Median Filtering Techniques For Removal of Impulse Noise From Digital Image, 2018 Conference on Emerging Devices and Smart Systems (ICEDSS). pp. 235-238.

Haaber, J., Cohn, M.T., Frees, D., Andersen, T.J., Ingmer, H., 2012. Planktonic aggregates of Staphylococcus aureus protect against common antibiotics. PLoS One 7(7), e41075.

Halder, S., Yadav, K.K., Sarkar, R., Mukherjee, S., Saha, P., Haldar, S., Karmakar, S., Sen, T., 2015. Alteration of Zeta potential and membrane permeability in bacteria: a study with cationic agents. Springerplus 4, 672.

Khoshmanesh, K., Baratchi, S., Tovar-Lopez, F.J., Nahavandi, S., Wlodkowic, D., Mitchell, A., Kalantar-zadeh, K., 2011. On-chip separation of Lactobacillus bacteria from yeasts using dielectrophoresis. Microfluidics and Nanofluidics 12(1-4), 597-606.

Larremore, D.B., Wilder, B., Lester, E., Shehata, S., Burke, J.M., Hay, J.A., Tambe, M., Mina, M.J., Parker, R., 2021. Test sensitivity is secondary to frequency and turnaround time for COVID-19 screening. Sci Adv 7(1).

Liaw, A., Wiener, M., 2002. Classification and regression by randomForest. R news 2(3), 18-22.

Lin, W.Y., Chen, C.H., Tseng, Y.J., Tsai, Y.T., Chang, C.Y., Wang, H.Y., Chen, C.K., 2018. Predicting post-stroke activities of daily living through a machine learning-based approach on initiating rehabilitation. Int J Med Inform 111, 159-164.

Lin, Y.-H., Lin, W.-Y., Lee, G.-B., 2009. Image-driven cell manipulation. IEEE Nanotechnology Magazine 3(3), 6-11.

Mikkaichi, T., Yeaman, M.R., Hoffmann, A., Group, M.S.I., 2019. Identifying determinants of persistent MRSA bacteremia using mathematical modeling. PLoS Comput Biol 15(7), e1007087.

Ohta, A.T., Chiou, P.-Y., Han, T.H., Liao, J.C., Bhardwaj, U., McCabe, E.R.B., Yu, F., Sun, R., Wu, M.C., 2007. Dynamic Cell and Microparticle Control via Optoelectronic Tweezers. Journal of Microelectromechanical Systems 16(3), 491-499.

Patel, P., Markx, G.H., 2008. Dielectric measurement of cell death. Enzyme Microb Tech 43(7), 463-470.

Rong, W., Li, Z., Zhang, W., Sun, L., 2014. An improved Canny edge detection algorithm, 2014 IEEE International Conference on Mechatronics and Automation. pp. 577-582.

Smith, A.R., 1978. Color gamut transform pairs. ACM SIGGRAPH Computer Graphics 12(3), 12-19.

Tseng, Y.-J., Huang, C.-E., Wen, C.-N., Lai, P.-Y., Wu, M.-H., Sun, Y.-C., Wang, H.-Y., Lu, J.-J., 2019. Predicting breast cancer metastasis by using serum biomarkers and clinicopathological data with machine learning technologies. International Journal of Medical Informatics.

Ventola, C.L., 2015. The antibiotic resistance crisis: part 1: causes and threats. P T 40(4), 277-283.

Wang, H.-Y., Chen, C.-Y., Chu, P.-Y., Zhu, Y.-X., Hsieh, C.-H., Lu, J.-J., Wu, M.-H., 2020a. Application of an optically induced dielectrophoresis (ODEP)-based microfluidic system for the detection and isolation of bacteria with heterogeneity of antibiotic susceptibility. Sensors and Actuators B: Chemical 307.

Wang, H.-Y., Lien, F., Liu, T.-P., Chen, C.-H., Chen, C.-J., Lu, J.-J., 2018. Application of a MALDI-TOF analysis platform (ClinProTools) for rapid and preliminary report of MRSA sequence types in Taiwan. PeerJ 6.

Wang, H.-Y., Lu, K.-P., Chung, C.-R., Tseng, Y.-J., Lee, T.-Y., Horng, J.-T., Chang, T.-H., Wu, M.-H., Lin, T.-W., Liu, T.-P., Lu, J.-J., 2020b. Rapidly predicting vancomycin

643 resistance of Enterococcus faecium through MALDI-TOF MS spectra obtained in
644 real-world clinical microbiology laboratory. Nature Communications.
645 Wang, H.Y., Chen, C.H., Lee, T.Y., Horng, J.T., Liu, T.P., Tseng, Y.J., Lu, J.J., 2018a. Rapid
646 Detection of Heterogeneous Vancomycin-Intermediate Staphylococcus aureus
647 Based on Matrix-Assisted Laser Desorption Ionization Time-of-Flight: Using a
648 Machine Learning Approach and Unbiased Validation. Front Microbiol 9, 2393.
649 Wang, H.Y., Chen, C.H., Shi, S., Chung, C.R., Wen, Y.H., Wu, M.H., Lebowitz, M.S., Zhou,
650 J., Lu, J.J., 2020a. Improving Multi-Tumor Biomarker Health Check-up Tests with
651 Machine Learning Algorithms. Cancers (Basel) 12(6).
652 Wang, H.Y., Chung, C.R., Wang, Z., Li, S., Chu, B.Y., Horng, J.T., Lu, J.J., Lee, T.Y.,
653 2020b. A large-scale investigation and identification of methicillin-resistant
654 Staphylococcus aureus based on peaks binning of matrix-assisted laser desorption
655 ionization-time of flight MS spectra. Brief Bioinform.
656 Wang, H.Y., Hsieh, C.H., Wen, C.N., Wen, Y.H., Chen, C.H., Lu, J.J., 2016. Cancers
657 Screening in an Asymptomatic Population by Using Multiple Tumour Markers.
658 PLoS One 11(6), e0158285.
659 Wang, H.Y., Lee, T.Y., Tseng, Y.J., Liu, T.P., Huang, K.Y., Chang, Y.T., Chen, C.H., Lu, J.J.,
660 2018b. A new scheme for strain typing of methicillin-resistant Staphylococcus
661 aureus on the basis of matrix-assisted laser desorption ionization time-of-flight mass
662 spectrometry by using machine learning approach. PLoS One 13(3), e0194289.
663 Wang, Z., Wang, H.Y., Chung, C.R., Horng, J.T., Lu, J.J., Lee, T.Y., 2020. Large-scale mass
664 spectrometry data combined with demographics analysis rapidly predicts methicillin
665 resistance in Staphylococcus aureus. Brief Bioinform.
666 Ward, A.C., Hannah, A.J., Kendrick, S.L., Tucker, N.P., MacGregor, G., Connolly, P., 2018.
667 Identification and characterisation of Staphylococcus aureus on low cost screen
668 printed carbon electrodes using impedance spectroscopy. Biosens Bioelectron 110,
669 65-70.
670 Welker, M., van Belkum, A., 2019. One System for All: Is Mass Spectrometry a Future
671 Alternative for Conventional Antibiotic Susceptibility Testing? Front Microbiol 10,
672 2711.
673 Wu, M.-H., Wang, H.-Y., Tai, C.-L., Chang, Y.-H., Chen, Y.-M., Huang, S.-B., Chiu, T.-K.,
674 Yang, T.-C., Wang, S.-S., 2013. Development of perfusion-based microbioreactor
675 platform capable of providing tunable dynamic compressive loading to 3-D cell
676 culture construct: Demonstration study of the effect of compressive stimulations on
677 articular chondrocyte functions. Sensors and Actuators B: Chemical 176, 86-96.
678 Xu, J., Li, F., Leier, A., Xiang, D., Shen, H.H., Marquez Lago, T.T., Li, J., Yu, D.J., Song, J.,
679 2021. Comprehensive assessment of machine learning-based methods for predicting
680 antimicrobial peptides. Brief Bioinform.

Xu, T., Han, X., Zhu, P., Dai, J., Liu, M., Liu, Y., Xu, J., Ma, B., 2021. A milliliter to picoliter-level centrifugal microfluidic concentrator for fast pathogen detection and antimicrobial susceptibility testing. Sensors and Actuators B: Chemical 343.

Yu, H., Jing, W., Iriya, R., Yang, Y., Syal, K., Mo, M., Grys, T.E., Haydel, S.E., Wang, S., Tao, N., 2018. Phenotypic Antimicrobial Susceptibility Testing with Deep Learning Video Microscopy. Anal Chem 90(10), 6314-6322.

Yu, J.-R., Chen, C.-H., Huang, T.-W., Lu, J.-J., Chung, C.-R., Lin, T.-W., Wu, M.-H., Tseng, Y.-J., Wang, H.-Y.

Zheng, E.J., Stokes, J.M., Collins, J.J., 2020. Eradicating Bacterial Persisters with Combinations of Strongly and Weakly Metabolism-Dependent Antibiotics. Cell Chem Biol.